5th International Conference on Biaxial/Multiaxial Fatigue and Fracture
Cracow'97, Poland

*Masao SAKANE, **Takamoto ITOH, *Seiji KIDA, *Masateru OHNAMI
***Darrell F. SOCIE

Dislocation Structure and Non-Proportional Hardening of Type 304 Stainless Steel

* *Department of Mechanical Engineering, Faculty of Science and Engineering, Ritsumeikan University, Nojihigashi Kusatsu-shi Shiga, Japan*
** *Department of Mechanical Engineering, Faculty of Engineering, Fukui University, Fukui,, Japan.*
*** *Department of Mechanical and Industrial Engineering, University of Illinois, Urbana, USA*

Key Words : Dislocation structure, Nonproportional loading, Stacking fault, Additional hardening

Abstract *:This paper describes the microstructure of Type 304 stainless steel after cyclic loading at room temperature under tension-torsion nonproportional strain paths. The degree of cyclic nonproportional hardening is correlated with changes in the dislocation substructure. Dislocation cells, dislocation bundles, twins and stacking faults are all observed. The type of microstructure formed and resultant stress response is dependent on the degree of nonproportional loading and strain range. Cyclic stress range was uniquely correlated with mean cell size.*

Notation

$\varepsilon_1(t)$	Maximum principal strain at time t
$\varepsilon_3(t)$	Minimum principal strain at time t
$\varepsilon_I(t)$	Maximum absolute value of the principal strain at time t : Max $\{\varepsilon_1(t), \varepsilon_3(t)\}$
$\varepsilon_{I\,max}$	Maximum value of $\varepsilon_I(t)$ in a cycle
$\Delta\varepsilon_I$	Maximum principal strain range under nonproportional straining
$\Delta\varepsilon_{NP}$	Nonproportional strain range
$\sigma_1(t)$	Maximum principal stress at time t
$\sigma_3(t)$	Minimum principal stress at time t
$\sigma_I(t)$	Maximum absolute value of the principal stress at time t : Max $\{\sigma_1(t), \sigma_3(t)\}$
$\Delta\sigma_I$	Maximum principal stress range under nonproportional straining
$\xi(t)$	Angle between the principal strain directions of $\varepsilon_1(t)$ and $\varepsilon_{I\,max}$
f_{NP}	Nonproportional factor
α	Material constant which expresses the amount of additional hardening
N_f	Number of cycles to failure

Introduction

Many practical applications such as the nuclear vessel of a fast breeder reactor have nonproportional stresses and strains under the combination of thermal and mechanical loading. Type 304 stainless steel is known as a material which shows a significant additional cyclic hardening under nonproportional loading in comparison with proportional loading. Recent studies have shown that the degree of the additional cyclic hardening is material dependent. Doong et. al. [1] reported the relationship between the microstructure and additional cyclic hardening behavior of 1100 aluminum alloy, oxygen free pure copper and Type 304 and 310 stainless steels. They reported that no additional hardening occurred in aluminum alloy but significant additional hardening in stainless steel. Nonproportional cyclic hardening was reported for pure copper. They discussed the microstructure change with proceeding cycles in detail for a limited number of strain paths. Cailletaud et. al. [2] compiled much of the published data and concluded that the main parameter governing the degree of nonproportional hardening in solid solution materials is the ease of cross slip. Itoh et. al.[3,4] studied nonproportional cyclic hardening of Type 304 stainless steel, pure copper, pure nickel, pure aluminum and 6061-T6 aluminum and reported that the degree of additional cyclic hardening is related to the stacking fault energy of the material. For a material with a low stacking fault energy such as Type 304 stainless steel, planar slip occurs and results in a large amount of additional cyclic hardening. This is caused by the interaction of many slip systems. Materials with a high stacking fault energy such as pure aluminum and 6061-T6 aluminum alloy deform by wavy slip. These materials do not show additional cyclic hardening during nonproportional loading The difference in the additional hardening behavior between high and low stacking fault energy materials is be related to the microstructure of the material but extensive and systematic studies have not yet been reported.

Several investigators have examined the dislocation structure for room temperature tests. Doquet[5] reported twin deformation as a primary deformation mechanism under nonproportional loading for binary Co33Ni. She reported that the increase in the amount of twin deformation is a cause of additional cyclic hardening during nonproportional loading. Jiao et. al. [6] examined alloy 800 H and observed deformation twins and suggested that the formation of twins depends not only on the shear stress but also on the normal stress acting on

the slip plane. McDowell et. al. [7] found that the hetrogeneity of ε-martensite and other planar slip deformation products (e.g. α' martensite) are a function of the nonproportionality in 304 stainless steel. They found that the homogeneity and morphology of the deformation products is of key importance. Cailletaud et. al. [1] observed ladders, veins or dislocation cell structures with loose outlines in uniaxial specimens but walls, mazes, cells, and , above all, abundant micro-twinning for nonproportionally loaded specimens of Type 316 stainless steel. Twinning is not an easy deformation mode in 316 steel at room temperature. The critical shear stress needed to induce twinning was reached because of the additional hardening during the nonproportional tests. Doong et. al. [1] found single slip structures under proportional loading of both 304 and 310 stainless steels. Multi-slip structures such as cells and labyrinths were found for nonproportional loading. At high temperatures, Nishino et. al. [8] observed the dislocation structure of Type 304 stainless steel cyclically loaded at 823 K and have discussed the relationship between the dislocation structure and hardening behavior. They concluded that anisotropic hardening is caused by the directionally developed cell formation and isotropic hardening by the formation of round-shaped cells.

Microstructural studies of additional nonproportional cyclic hardening have been limited to a small number of strain paths so that the results of these studies are rather qualitative. Little quantitative discussion has been reported. This paper studies the microstructure and cyclic stress-strain relationships obtained at room temperature under 14 nonproportional strain paths for Type 304 stainless steel, and will discuss the relationship between stress response and cell structure quantitatively.

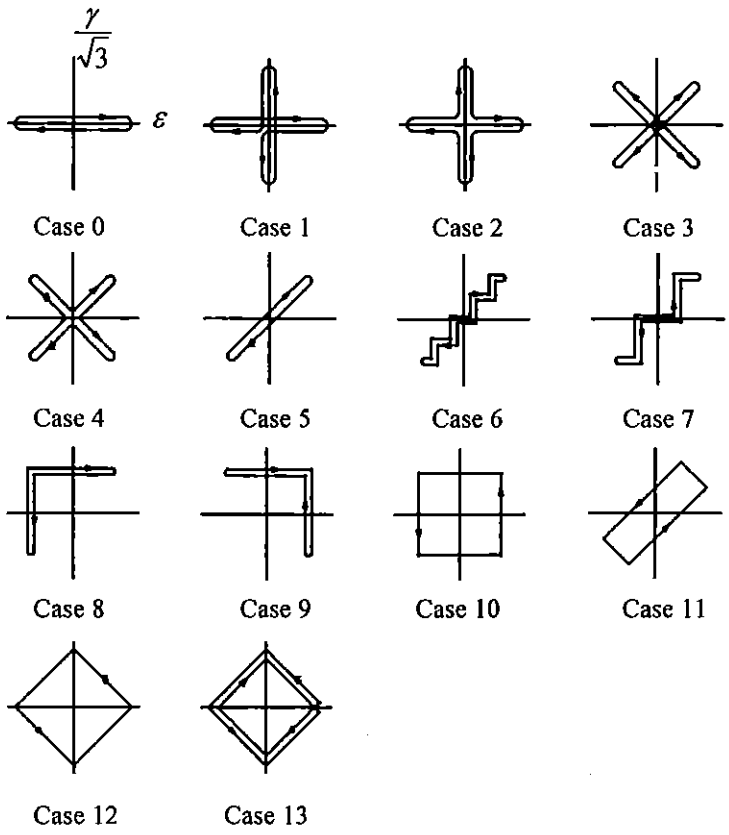

Fig.1 Proportional and nonproportional loading paths.

Experimental Procedure

The material tested is Type 304 stainless steel which received a solution treatment at 1373 K for one hour. Hollow cylindrical specimens with 9 mm I.D., 12 mm O.D., and 4.6 mm gage length were employed in this study. Strain controlled cyclic loading tests at a Mises' effective strain rate of 0.1 %/sec were carried out at ambient temperature. Testing details are reported by Itoh et. al. [9]. Figure 1 shows the 14 proportional and nonproportional loading histories employed, where ε and γ are the axial and shear strains, respectively. Case 0 is a push-pull proportional test which is the basic data for examining the microstructure. Case 0 testing was carried out at strain ranges between 0.5 and 1.5 %. Case 5 is also a proportional test as is Case 0, but is a combined push-pull and reversed torsion test. The other Cases are nonproportional tests in which the severity of nonproportional loading is determined by the strain history. In all the tests except

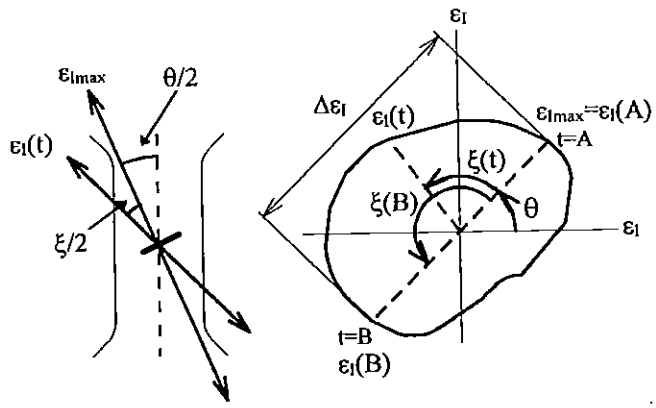

Fig.2 Definition of maximum principal strain range under nonproportional loading.

for Case 0, axial and shear strain ranges were 0.5 and 0.8 % Mises' equivalent strain.

One cycle is defined here as a full straining for both axial and shear strain. All the tests except Cases 3, 4 and 13 were counted as one cycle and these tests were counted as two cycles for a full straining along the strain path chosen in Fig. 1. The number of cycles to failure (N_f) was defined as the cycle at which the axial stress amplitude decreased to 5 percent of the saturation stress in tension.

After the cyclic loading tests, thin foils of 3 mm diameter were cut from specimens away from cracks by a wire cutter to observe the microstructure. They were polished down to about 0.2 mm in thickness with emery papers and were jet-electropolished in acetate perchlorate. A JEOL JEM-100C (100kV) was used to observe the microstructure and diffraction pattern.

Definition of principal strain and stress ranges and nonproportional parameter

During nonproportional loading, stress and strain amplitudes vary with time, so that the principal strain and stress ranges must be defined. In a previous paper [9] , the authors have proposed a definition of the maximum principal strain and stress ranges for nonproportional loadings and this paper follows that definition.

The maximum principal strain range, $\Delta\varepsilon_I$, is defined as,

$$\Delta\varepsilon_I = Max\left[\varepsilon_{1max} - \cos(\xi(t))\cdot\varepsilon_I(t)\right] \tag{1}$$

In this equation, $\varepsilon_1(t)$ is the maximum absolute value of principal strain at time t and

$$\begin{aligned}\varepsilon_I(t) &= |\varepsilon_1(t)| \quad for\ |\varepsilon_1(t)| \geq |\varepsilon_3(t)| \\ \varepsilon_I(t) &= |\varepsilon_3(t)| \quad for\ |\varepsilon_1(t)| \leq |\varepsilon_3(t)|\end{aligned} \tag{2}$$

where $\varepsilon_1(t)$ and $\varepsilon_3(t)$ are the maximum and minimum principal strains at time t, respectively. Figure 2 is a polar figure of $\varepsilon_1(t)$ schematically showing $\varepsilon_1(t)$, $\xi(t)$ and $\Delta\varepsilon_I$. In equation (1), ε_{1max} is the maximum value of $\varepsilon_1(t)$ in a cycle and $\xi(t)$ is the angle between ε_{1max} and $\varepsilon_1(t)$ directions. Thus, $\Delta\varepsilon_I(t)$ is determined by the two strains, $\varepsilon_1(A)$ and $\varepsilon_1(B)$, and by the angle between the two strain directions in Fig. 2, where A is the time giving ε_{1max} and B the time maximizing the strain range in equation 1.

The maximum principal stress range, $\Delta\sigma_I(t)$, has a similar definition to $\Delta\varepsilon_I$,

$$\begin{aligned}\Delta\sigma_I &= \sigma_I(A) - \cos(\xi(B))\cdot\sigma_I(B) \\ \sigma_I(t) &= |\sigma_1(t)| \quad for\ |\sigma_1(t)| \geq |\sigma_3(t)| \\ \sigma_I(t) &= |\sigma_3(t)| \quad for\ |\sigma_1(t)| \leq |\sigma_3(t)|\end{aligned} \tag{3}$$

where $\sigma_1(t)$ and $\sigma_3(t)$ are the maximum and minimum principal stresses, respectively. The two times A and B correspond with those defined for the maximum principal strain range.

A nonproportional factor, f_{NP}, was proposed by the authors to express the severity of nonproportional loading [6].

$$f_{NP} = \frac{\pi}{2T\varepsilon_{1max}}\int_0^T (|\sin(\xi(t))|\cdot\varepsilon_I(t))dt \tag{4}$$

where T is the time for a cycle shown in Fig. 1. The value of f_{NP} is zero under proportional loading and is the range of $0 \leq f_{NP} \leq 1$ under nonproportional loading. As shown in equation 4, f_{NP} is a function of only the applied strain history to avoid the need to compute stresses and plastic strains.

The authors [9] have proposed the following strain parameter to correlate nonproportional LCF lives,

$$\Delta \varepsilon_{NP} = (1 + \alpha \cdot f_{NP}) \cdot \Delta \varepsilon_1 \tag{5}$$

where α is a material parameter related to the additional hardening of the material under nonproportional loading, and α is defined as the ratio of stress range under nonproportional circular loading in $\gamma/\sqrt{3}$-ε plot to that under proportional loading at the same Mises equivalent strain. The value of α becomes larger for lower stacking fault energy materials [1-4]. Murakami et. al. [10] showed that this parameter will decrease with increasing temperatures. For Type 304 stainless steel at room temperature, α takes the value of 0.9. Benallal and Marquis[11] show a small strain range dependance of α but here we take it as a constant. The term $(1+\alpha \cdot f_{NP})$ accounts for the additional cyclic hardening observed during nonproportional cyclic loading and is similar to damage parameters that are based on the product of stress and strain range. The advantage of this parameter is that it does not require a sophisticated transient cyclic plasticity model to obtain the stress ranges.

Experimental Results and Discussion

A complete tabular listing of all test data is available in [9] but the test data is not presented here because of the space of the paper. Fatigue lives for Cases 0-13 significantly depend on the strain history. Rotating principal strain directions in tests such as Cases 8-10, 12 and 13 yields the largest reduction in fatigue lives by as much as a factor of 10. In Cases 6-9, steps in the path can have a large influence on fatigue lives when the number of steps is small and the path length is large. Thus, Case 6 shows a small reduction in fatigue life as the strain history is nearly proportional loading because of the small step length. Figure 3 correlates LCF lives with principal stress range. The figure shows that a significant additional hardening occurs under nonproportional loadings. Greater additional cyclic hardening results in smaller fatigue lives. Thus, an estimate of additional hardening is necessary for predicting fatigue lives under nonproportional loading in the LCF regime. Figure 4 correlates the nonproportional LCF lives with equivalent strain given in equation 5. Most of the data are correlated within a factor of two scatter band.

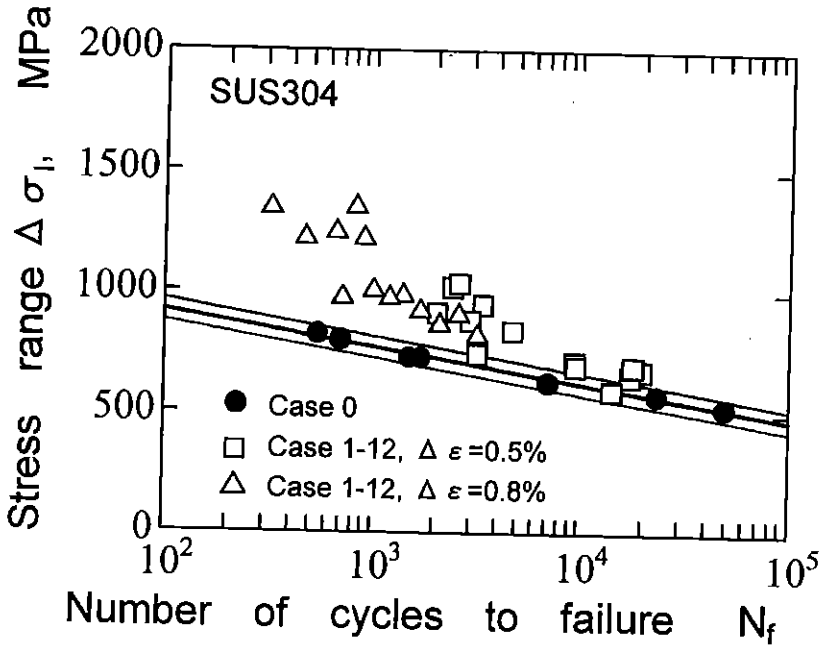

Fig.3 Correlation of nonproportional fatigue lives with principal stress.

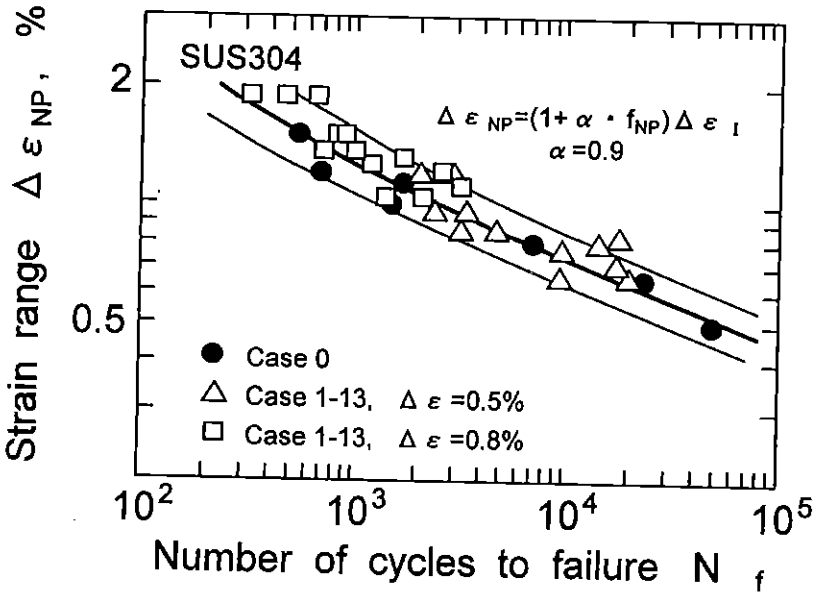

Fig.4 Correlation of nonproportional fatigue lives with nonproportional strain in Eq.5.

Figure 5 shows the relationship between the stabilized axial and shear stresses for twelve of the fourteen loading histories. The stress response for Case 8 is the mirror image of Case 9 and was omitted from the figure. In the figures, dashed lines are the results at $\Delta\varepsilon = 0.5$ %, and solid lines are the results at $\Delta\varepsilon = 0.8$ %. The shear stress scale has been plotted as one half of the axial stress scale so that stresses can easily be compared on the basis of maximum shear stress. Comparing the equivalent stresses for Cases 1 and 2 with Case 0 at $\Delta\varepsilon = 0.5$ and 0.8 % shows significant nonproportional hardening due to the change of principal strain direction at zero strain. The normal stress - shear stress relationship of Case 1 is different from that of Case 2 which shows that a fully reversed straining has a different influence on stress response from a zero-to-maximum straining, and the former strain history causes greater additional hardening than the latter one. This additional hardening also results in a lower fatigue life for Case 2. The shape of the τ - σ plot of Cases 3 and 4 is similar to that of Cases 1 and 2, respectively, after giving a rotation of 45 degrees to the former two cases. However, the stress amplitude of Cases 3 and 4 is larger than that of Cases 1 and 2 because the shear and axial strains are applied simultaneously resulting in a cyclic strain range in the former two cases that is larger by about 1.4 times.

A simple method for visualizing degree of nonproportionality is useful when interpreting the stresses in Fig. 5. If an ellipse is drawn so as to circumscribe the entire stress path, nonproportionality can be thought of as the ratio of the minor axis to the major axis. In Case 5, the minor axis of an ellipse circumscribing the loading history is small corresponding to a low degree of nonproportionality. The degree of nonproportionality increases in going from Case 5 to Case 10. This is easily visualized as an increasingly circular ellipse circumscribing the stress history. The size of the ellipse also increases as the degree of nonproportionality increases. Case 5 is proportional loading where the normal stress amplitude σ is same as the shear stress amplitude $\sqrt{3}\tau$ since the normal strain equals the shear strain on Mises basis. Comparing the stress response in Fig. 5 of Case 5 with that of Cases 6, 7 and 8 shows that the normal and shear stress amplitudes are larger as the degree of nonproportionality increases. Fatigue lives tend to decrease as these stresses increase.

Comparison of the stress response between Cases 5, 11 and 12 illustrates the effect of loading phase between the normal and shear strains. A linear stress-strain relationship is obtained on τ - σ plot for Case 5, but a box τ-σ relationship is found for Cases 11 and 12. The normal and shear

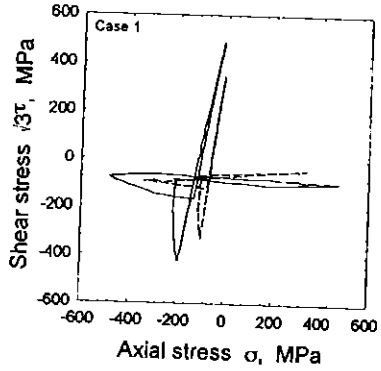

(a) Case 1

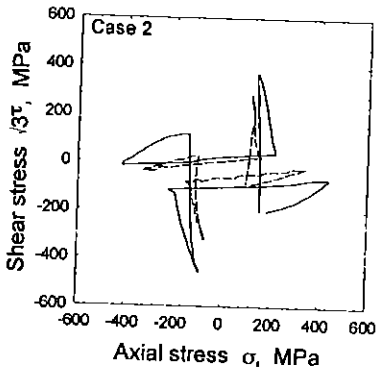

(b) Case 2

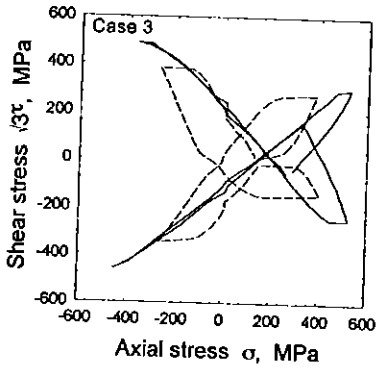

(c) Case 3

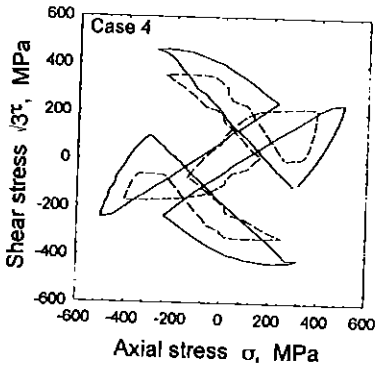

(d) Case 4

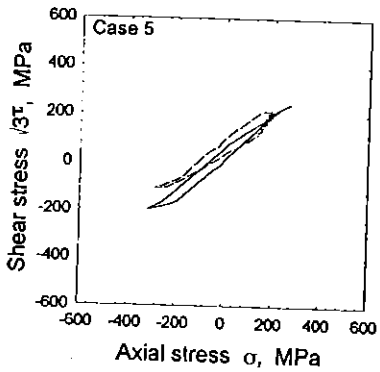

(e) Case 5

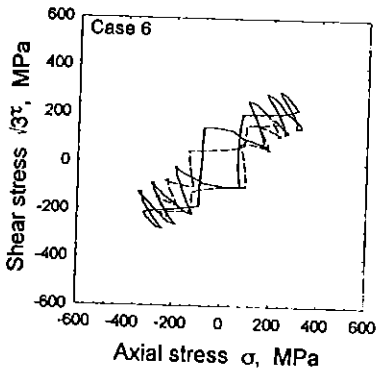

(f) Case 6

Fig.5 Correlation between normal and shear stresses under nonproportional loading. (dotted line : $\Delta\varepsilon$ =0.5%, solid line : $\Delta\varepsilon$ =0.8%)

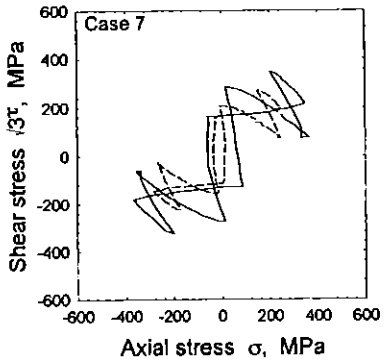

(g)Case 7

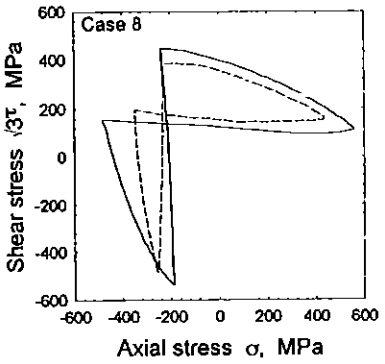

(h) Case 8

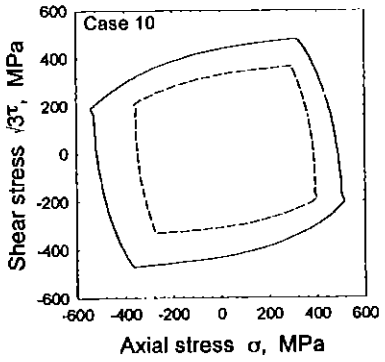

(i) Case 10

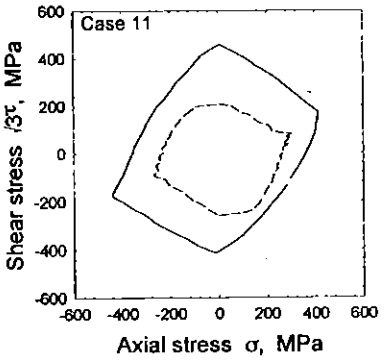

(j) Case 11

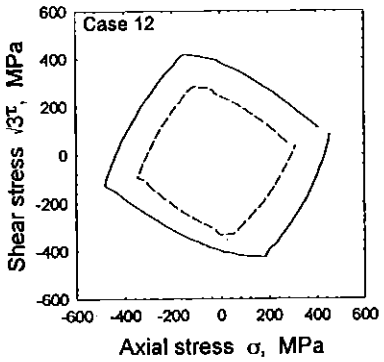

(k) Case 12

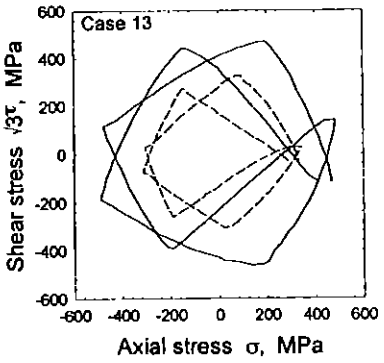

(l) Case 13

Fig.5 Correlation between normal and shear stresses under nonproportional loading. (dotted line : $\Delta\varepsilon$ =0.5%, solid line : $\Delta\varepsilon$ =0.8%)

stress ranges in Cases 11 and 12 are significantly larger than those of Case 5 and the stresses in Case 12 are somewhat larger than in comparison with Case 11. The principal strain amplitude of Case 12 is smaller than that of Case 11. This indicates that the 90-degrees phase difference has a greater hardening effect than a 45-degrees phase difference. Case 13 exhibits a much more significant additional hardening than Case 12, which indicates that the turn around of straining increases the additional hardening effect.

Cases 8, 9 and 10 give the largest additional hardening among the 13 strain paths. A 40 - 60 % normal stress increase is found in these three strain paths in comparison with the Case 0 test. Socie [12] has reported the circular strain path has a more pronounced additional hardening than the box strain path for this material where a 90 % stress increase was found in the circular strain path.

Observations of Dislocation Structure

Additional hardening has been reported to have a close connection with dislocation structure [9], but there have been few systematic and quantitative studies of the relationship between the microstructure and additional hardening. Figures 6 (a)-(j) show the microstructure observed by TEM. Figure 6 (a) shows the dislocation structure before testing where the dislocation density is very low and no specific substructure is identified.

A cell structure is observed in Case 0, Fig. 6 (b), where the mean cell diameter is around 1μm. Cell formation was also observed in the specimens cyclically loaded at large strain ranges (> 1%) in Case 0. Dislocation bundles which indicates the cluster of dislocations were observed at low strain ranges (< 0.8 %) in Case 0.

Cell structures, twins and stacking faults were observed in Case 1, Fig.6 (c), but only twins and stacking faults were observed in Case 3, Fig.6 (d). No clear cell formation was found in Case 3, and dislocation bundles were observed. Many stacking faults occurred before cell formation and they appear to hinder the cell formation in Case 3. The number of stacking faults in Case 3 is larger than that in Case 1. The phasing of the applied strains produces larger stress and strain ranges for Case 3.

Nishino et. al.[8] reported that a ladder or maze structure was a common structure for Type 304 stainless steel in proportional straining and a cell structure was primarily found in the nonproportional straining like Case 1 at high temperature. At room temperature, however, cell

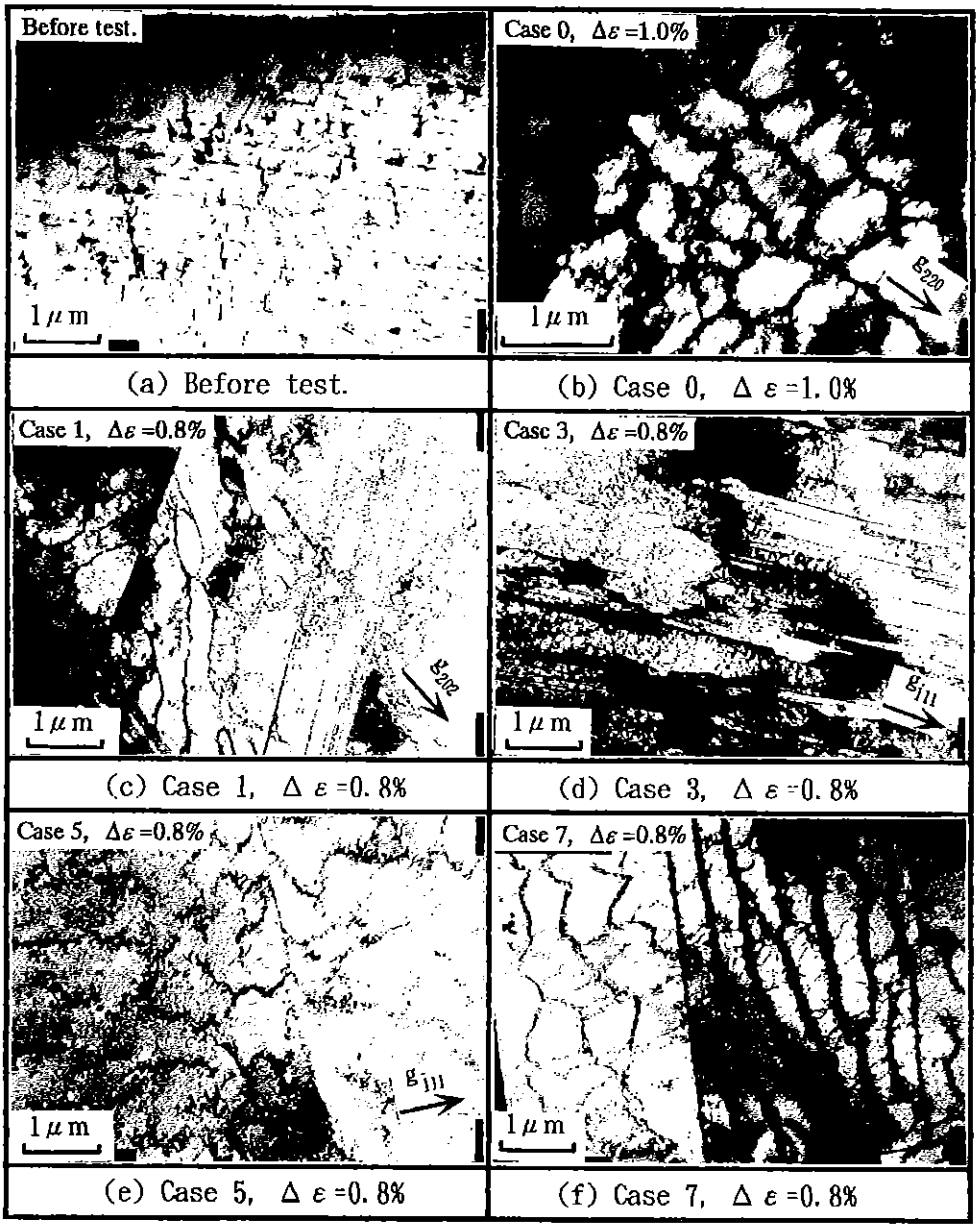

Fig.6 Microstructure observed by SEM.

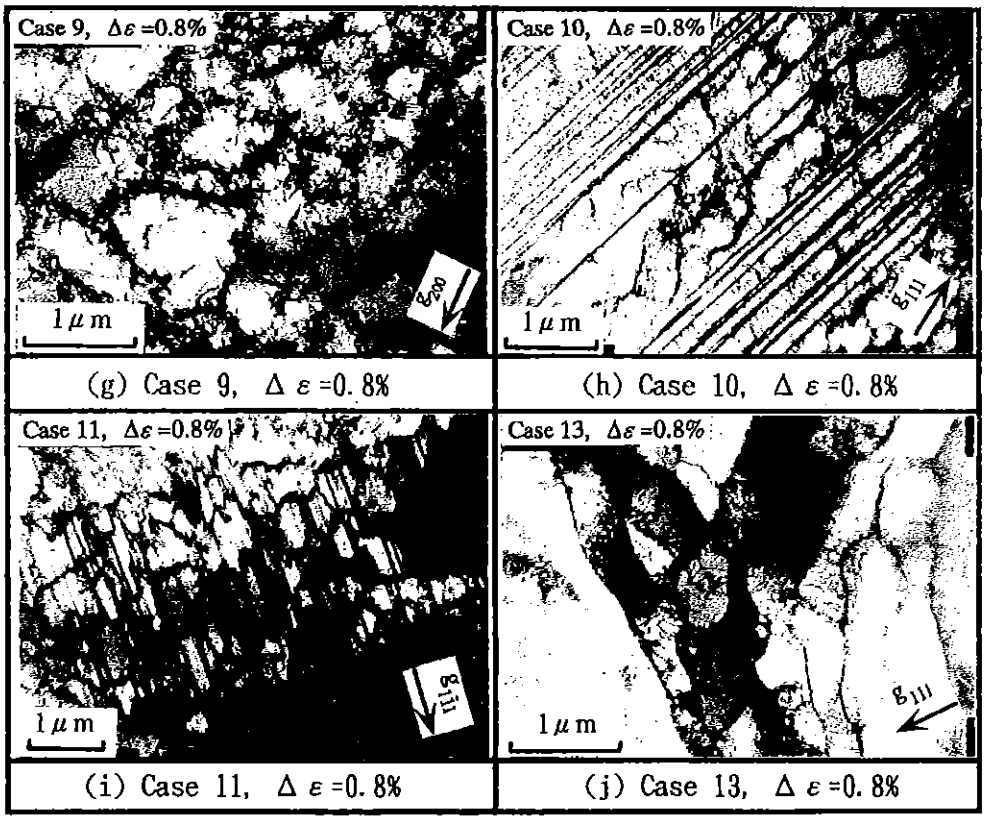

Fig.6 Microstructure observed by SEM.

structures formed and no ladder or maze structures were observed in Case 0 loading. This difference in dislocation structure between room and elevated temperatures results from the difference in the thermal activation. At elevated temperatures, dislocations glide more easily to form a structure of low elastic energy by the assistance of thermal activation so that a ladder or maze structure, which is a lower elastic energy microstructure than the cell, was found. In Case 5, which is a proportional straining, Fig.6 (e), cell structures were observed. A twin boundary was also observed at the center of the photograph. Case 7, Fig. 6(f), exhibits a clear twin boundary at the center of the photograph. Dislocation walls are observed in the right of the photograph, and a cell structure is found in the left of the photograph. In Case 7, columnar cells were formed and Fig.6 (f) shows the two different sections of the columnar grains; the left is the normal section to columnar axes and the right is the parallel section of them. In Case 7, the maximum shear strain direction changed its direction, so that dislocations would easily rearrange

to columnar structure by the cross steps.

Cases 5 - 10 all have the same maximum shear strain ranges. Cases 8 - 10 have a rectangular or box strain history. In these strain paths, the maximum shear strain direction rotates continuously, so that many slip systems operate. The additional hardening was most significant in these strain paths. Cases 11 -13 are also rectangular strain paths but the phasing of the strains is such that the maximum shear strain range is smaller than Cases 5 - 10. In Case 9, Fig.6 (g), cell boundaries are not clear, but many dislocations exist even in the cells. The maximum shear stress direction rotates continuously in Case 9, so many slip planes operate and interact, and which results in the significant additional hardening.

In Cases 10 and 11, Figs.6 (h) and (i), many stacking faults were observed. Since Type 304 stainless steel is a material of low stacking fault energy, slip is planar and there are many partial dislocations which make a stacking fault between them. Long stacking faults exceeding several subgrains in length were formed in Case 10 with short stacking faults formed within cells in Case 11. The long stacking faults were formed by the severe box nonproportional straining and which hindered the cell formation, while, in Case 11, the cells were formed earlier than the stacking faults and stacking faults were stopped by the cell boundaries.

For Case 13, Fig.6 (j), the principal stress range in Case 13 is larger than that of Case 9, so that cell structure of Case 13 is different from Case 9. For Case 13, fine cells are found and they are rather close to subgrain since the cell boundaries are rigid and misorientation angle between cells is rather large. This strain path made resulted in clear cells and rigid cell boundaries.

Figure 7 is a microstructure map showing the cell, dislocation bundle and stacking fault boundaries as functions of maximum principal strain range and nonproportional factor for all the strain paths. In the figure, solid symbols indicate tests in which only cells were observed, while open symbols represent tests in which cells and other dislocation structures were found. Asterisks indicate tests where stacking faults were observed and the number at the data indicates the strain path number shown in Fig.1.

This figure shows that stacking faults were observed in almost all the tests and did not depend on the principal strain range and nonproportional factor. Type 304 is a low stacking fault energy material and a dislocation easily splits into partial dislocations, making a staking fault between them. A partial dislocation glides on the slip plane, and a stacking fault arises between the partial dislocations. Many stacking faults seem to be generated by this mechanism.

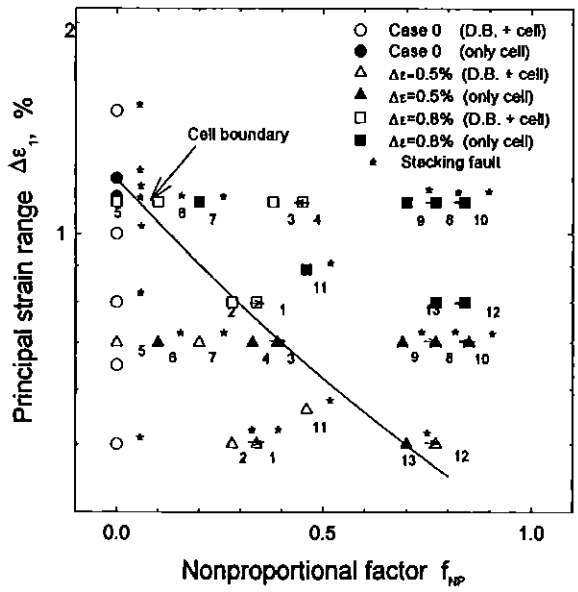

Fig.7 Relationship between microstructure, maximum principal strain range and nonproportional factor.

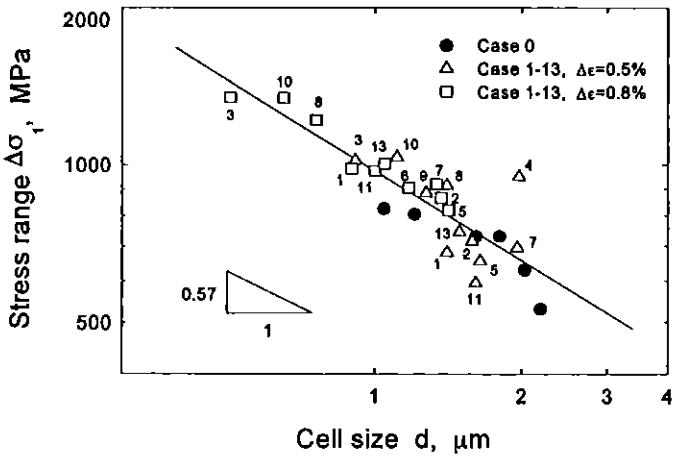

Fig.8 Correlation between mean cell size and principal stress range.

There is a critical combination of strain range and nonproportional factor for forming cells indicated by the solid line. In the region above the line, the microstructure is only cells but other microstructures together with cells were observed for the test conditions below the solid line. Figure 8 shows the relationship between the mean cell size and the maximum principal stress range for all the tests where the cell structure was observed. The mean cell size was determined by the Heyn method (JIS G0552), observing 3 or 4 locations of each specimen. Maximum principal stress range and mean cell size can be approximated by a straight line for all of the strain histories. The relationship is,

$$\Delta\sigma = m \times d^{n} \tag{8}$$

The values of m and n are 975 MPa and -0.57, respectively when d is measured in μm. The value of exponent is close to -1/2, so that the Hall-Petch relationship holds in proportional and nonproportional loadings. As shown in Fig.7, various microstructures are formed under nonproportional loading. However, the results in Fig.8 indicates that the additional hardening in nonproportional loading is mainly caused by reduction of cell size. The severe interaction of slip systems under nonproportional loading reduces the cell size and results in the additional hardening. The results also imply that microstructures other than cell structure have almost no influence on the additional hardening.

Conclusions

(1) Dislocation substructures observed under nonproportional loading were associated with cells, stacking faults, twins and bundles.

(2) A microstructure map was proposed that shows conditions for forming cells and stacking faults as functions of the maximum principal strain range and a nonproportional factor. There exists a critical boundary for forming cells. Stacking faults were observed in almost all the proportional and nonproportional tests.

(3) The principal stress range was uniquely correlated with the mean cell size and is independant of the strain loading path which indicates that the additional hardening was mainly associated with a reduction of cell size.

References

(1) Doong, S. H., Socie, D. F. and M.Robertson, I., (1990), Dislocation Substructure and Nonproportional Hardening, *Journal Engineering Materials Technology*, Vol. 112 -4, pp.456-465.

(2) Cailletaud, G., Doquet ,V. and Pineau, A.,(1991) , Cyclic Multiaxial Behavior of an Austenitic Stainless Steel: Microstructural Observations and Macromechanical Modeling, *Fatigue Under Biaxial and Multiaxial Loading*, ESIS 10, ed. Kussmaul et. al. , pp.131-149.

(3) Itoh, T., Sakane, M., Ohnami, M. and Ameyama, K.,(1992), Effect of Stacking Fault Energy on Cyclic Constitutive Relation Under Nonproportional Loading, *Journal of The Society of Materials Science, Japan*, Vol.41-468, pp.1361-1367 (in Japanese).

(4) Itoh, T., Sakane, M., Ohnami, M. and Ameyama, K., (1992), Additional Hardening due to Nonproportional Cyclic Loading - A Contribution of Stacking Fault Energy, *MECAMAT'92, Proceedings International Seminar on Multiaxial Plasticity, Cachan, France* (Benallal *et. al.*, eds.), pp.43-50.

(5) Doquet, V.,(1992), Deformation Twinning and Cyclic Behavior of A CoNi Alloy Under Multiaxial Loading, *MECAMAT'92, Proceedings International Seminar on Multiaxial Plasticity, Cachan, France*, pp.51-66.

(6) Jaio, F., Osterle, W., Portella, P.D. and Ziebs, J., (1995), Biaxial Path Dependance of Low Cycle Fatigue Behavior and Microstructure of Alloy 800 H at Room Temperature, *Materials Science and Engineering*, Vol.A196, pp.19-24.

(7) McDonnell, D.L., Stahl, D.R., Stock, S.R. and Antolovich, S.D., (1988), *Biaxial Path Dependance of Deformation Substructure of Type 304 Stainless Steel*, Metallurgical Transactions A, Vol.19A, pp.1277-1293.

(8) Nishino, S., Hamada, N., Sakane, M., Ohnami, M., Matsumura, N. and Tokizane, M.,(1986), Microstructural Study of Cyclic Strain Hardening Behavior in Biaxial Stress State at High Temperature, *Fatigue and Fracture of Engineering Materials and Structure*, Vol.9-1, pp.65-77.

(9) Itoh, T., Sakane, M., Ohnami, M. and Socie, D. F., (1995), Nonproportional Low Cycle Fatigue Criterion for Type 304 Stainless Steel , *ASME Journal of Engineering Material and Technology*, Vol.117-3, pp.285 - 292.

(10) Murakami, S., Kawai, M., Aoki, K. and Ohmi, Y., (1989), Temperature Dependance of Multiaxial Non-Proportional Cyclic behavior of Type 316 Stainless Steel, *Journal Engineering Materials Technology*, Vol.111-1, pp.32-39.

(11) Benallal, A. and Marquis, D., (1987), Constitutive Equations for Nonproportional Cyclic Elasto-Viscoplasticity, *Journal Engineering Materials Technology*, Vol.109-4, 326-336.

(12) Socie, D.F., (1987), Multiaxial Fatigue Damage Models, *Journal Engineering Materials Technology*, Vol.109-3 , pp.293-298.

Acknowledgment The authors express their gratitude to Dr. Kei Ameyama, the associate professor of Ritsumeikan University, for assisting with the TEM observations.